Macromolecules

ARTICLE

pubs.acs.org/Macromolecules

Atomistic Study of Surface Effects on Polyelectrolyte Adsorption: Case Study of a Poly(styrenesulfonate) Monolayer

Baofu Qiao, Juan J. Cerdà, and Christian Holm*

Institute for Computational Physics, Universität Stuttgart, Pfaffenwaldring 27, 70569 Stuttgart, Germany

Supporting Information

ABSTRACT: Extensive all-atom molecular dynamics simulations have been performed to investigate the effect of surface features on the adsorption of poly(styrenesulfonate) (PSS) oligomers on top of a modified graphite substrate. In particular, we have investigated hydrophilic and hydrophobic model surfaces, accompanied by a variable surface charge density σ_s in the range 0−0.164 C/m^2. Our results demonstrate that short-range interactions originating from the adsorbing substrate play a significant role in the layer structure of the adsorbed PSS, and they alone are already sufficient to induce a stable PSS adsorption layer. The presence of additional hydrophilic hydroxyl groups and charges on the adsorbing surface can further enhance the adsorption of PSS sulfonate groups at lower σ_s, whereas for the case of σ_s = 0.164 C/m^2, the influence of the surface hydroxyl groups becomes negligible compared to that of the surface charges. The adsorbed PSS chains show mostly conformations where the PSS backbones are approximately parallel to the adsorbing surface. In some case, however, also the PSS backbones stand on top of the surface. Both the obtained surface charge overcompensation and the surface coverage are in good agreement with a previous experimental work [Ahrens et al. *Macromolecules* **2001**, *34*, 4504−4512]. Between the first PSS adsorption layer and the adsorbing substrate, we always find a water-rich region. The orientation of the water molecules in this region depends crucially on the features of the adsorbing surface. Our simulations suggest that the water-involved hydrogen bondings play a dominant role in determining the orientation of the water molecules. We also observe a decrease of the dielectric constant of water in the region close to the adsorbing surface in all of the investigated systems that is more pronounced for the hydrophilically modified surface and moreover increases with rising surface charge density. We suggest that this effect could lead to an electrostatic stabilization of the monolayer surface.

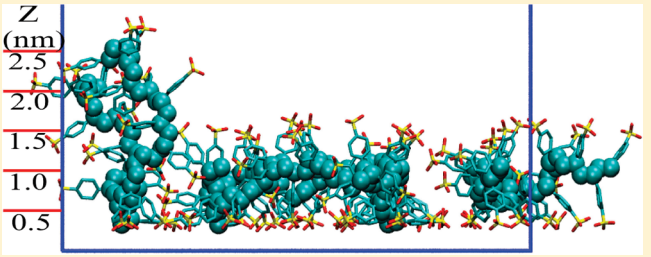

I. INTRODUCTION

The adsorption of polyelectrolytes (PEs) has been extensively investigated for several decades due to its significance in practical applications such as colloidal stabilization and coating. Reviews of the experimental, theoretical, and computational studies have been presented in refs 1−4. Recently, the developments in the field of polyelectrolyte multilayer (PEM), in particular thanks to the layer-by-layer deposition technique,[5,6] which involves an alternating deposition of polycation and polyanion layers onto a charged substrate, have revived the study on PE adsorption.

Despite the many advances, the current understanding of the mechanism of adsorption and of the microscopic structure of PEs after adsorption is still limited: nowadays, the experimental instruments are still limited to probe the structure beyond the length scale of tens of nanometers (see, e.g., refs 7 and 8), and the theoretical and computational works done so far are always involving some approximations. For the computational works, for instance, coarse-grained (CG) models, like the bead−spring model, are generally used due to the importance of Coulomb interaction in PEs. In the bead−spring model, several PE monomers are coarse-grained into one structureless bead, and the bonds between PE beads are modeled by a harmonic potential. Moreover, the solvent is usually treated implicitly. Despite their usefulness, the CG models might lead to different adsorption behavior of PEs from that observed in real experiment because of the lack of the details at the atomistic level. Reddy and Yethiraj,[9] by studying the adsorption of CG-level PEs using three different solvent models (one explicit and two implicit, modeled using structureless beads), have found that the treatment of the solvent is very important for the behavior of PE absorption. Under poor solvent condition, one thick PE layer can be formed on both charged and neutral surfaces when the explicit solvent model was applied, while neither of the two implicit solvent models leads to consistent observations. Therefore, they suggested that the solvent must be explicitly incorporated for accurate investigation of PE adsorption under poor solvent condition.[9]

Fortunately, due to the boost in computational capabilities of modern computers, it is nowadays feasible to investigate the adsorption of (oligomeric) PEs using atomistic level simulations. At the atomistic level description, atoms of the PEs and of the

Received: November 16, 2010
Revised: January 14, 2011
Published: February 09, 2011

solvent molecules are represented explicitly, bringing a higher resolution than CG models in both the polyelectrolyte and the solvent. Actually, previous work on PE adsorption at atomistic level exists: in ref 10 the adsorption of poly(styrenesulfonate) (PSS) (with Li^+ counterions) onto a graphite wall has been investigated at different surface charge densities, namely, $\sigma_s = 0$, 0.101, and −0.101 C/m^2. The interfacial structure of waters and PSS, and in particular the charge density profiles, were investigated in the presence of $BaCl_2$ or $LaCl_3$ multivalent salts. In ref 10, simulations of PSS oligomers (degree of polymerization (DP) 8) were performed at the united-atom level (i.e., the hydrogen atoms chemically bonded to carbon are represented implicitly by adjusting the force field parameters of such carbons to include the interactions originated from the implicit hydrogens).

Because of the limitation of experimental instruments, the number of publications in which the nature of the adsorbing surface is described explicitly is so far very scarce, even though surface features are expected to play an important role in the PE adsorption. Helm and co-workers[11] prepared positively charged diocatadecyldimethylammonium bromide (DODAB) monolayers as the liquid adsorbing substrate for the PSS adsorption. The surface charge density were in the range 0.08−0.32 C/m^2. In ref 12, the controlled and fixed surface charge density was experimentally obtained by the use of gold−thiol self-assembled monolayers by altering the concentration of $HS(CH_2)_{11}N^+(CH_3)_3$ in the deposition solution. The surface charge density was varied from 0 to 0.37 C/m^2 to investigate the adsorption of surfactant, sodium dodecyl sulfate. A spherical solid substrate of polystyrene latex particles was also employed for the PSS adsorption.[13] Such substrate was positively charged by 2,2′-azobis(2-methylpropionamidine) dihydrocholride, or negatively charged by potassium persulfate, with the surface charge density ranging from −0.03 to 0.03 C/m^2. Regarding computational investigations, only two works have been published so far to the best of our knowledge: one atomistic level[10] and one CG-level[14] simulations. In ref 14, the surface hydrophilicity/hydrophobicity, the density, and the distribution of the surface charges have been investigated, and the CG-level PE chains were deposited from the implicit solvent solution. The surface hydrophilicity/hydrophobicity feature was controlled by changing the interaction between the surface and the PE beads. The surface charges, in the density range of 0.07−0.58 e/δ^2 (where δ is the diameter of the PE beads), were uniformly or randomly distributed. The surface charge density of 0.58 e/δ^2 can be mapped to a physical system of 0.18 C/m^2.[15,16]

In order to provide further insight into this topic, all-atom (AA) molecular dynamics simulations are performed in the present work to study the adsorption of PSS depending on the surface features, namely, hydrophilicity/hydrophobicity and surface charge. The aim is to understand how the adsorption ability of PSS depends on the adsorbing surface features. This is expected to be useful in elucidating the buildup of PEMs. The present AA simulations could also be employed for some valuable information, such as substrate−PSS and PSS−PSS interaction energies, to further refine our CG models[16,17] on PEM investigation.

The rest of this work is organized as follows. In section II, the model and simulation details are described. The results obtained and the discussion on the adsorption behavior of PSS and water are presented in section III. Finally, some conclusions are given in section IV.

Table 1. Composition of the Systems

	adsorbing substrate				no. of components		
system[a]	wall[b]	ρ_{OH}[c]	σ_s[d]	Cl^-	PSS[e]	Na^+	H_2O
P.1	yes	19.1			21	252	32 760
P.2	yes	19.1	0.073	16	21	252	32 760
P.3	yes	19.1	0.164	36	21	252	32 760
H.1	yes				21	252	32 760
H.2	yes		0.073	16	21	252	32 760
H.3	yes		0.164	36	21	252	32 760
P.0	yes	19.1					32 760
H.0	yes						32 760
R.0[f]	no				21	252	32 760

[a] Systems labeled with P (H) represent those with hydrophilic (hydrophobic) adsorbing surface. [b] Implicit graphite wall described by Steele 10−4−3 wall potential. [c] Number density of surface hydroxyl groups in unit of nm^{-2}. [d] Surface charge density in unit of C/m^2. 0.073 and 0.164 C/m^2 correspond to uniformly distributed surface charges of 16 e (P.2, H.2) and 36 e (P.3, H.3), respectively. The counterions of the surface charges are Cl^-. [e] Degree of polymerization is 12. [f] Bulk PSSNa solution, which is simulated in NPT ensemble at ambient condition. See ref 26 for other simulation details.

II. SIMULATION METHODOLOGY

A. Adsorbing Substrate. To investigate the substrate effect on PSS adsorption, two kinds of substrates, one hydrophilic (P for short) and one hydrophobic (H for short), were prepared at $z = 0$. For each of them, three surface charge densities were employed, which in combination yield six different adsorbing substrates in total. See Table 1 for the complete information.

To speed up the very time-consuming simulations, an implicit structureless graphite wall is used to model the hydrophobic substrate. The interaction involving the implicit graphite wall has been described by the Steele 10−4−3 wall potential:[19−21]

$$U_{sf}(z) = 2\pi\rho_s\Delta\varepsilon_{sf}\sigma_{sf}^2\left\{\frac{2}{5}\left(\frac{\sigma_{sf}}{z}\right)^{10} - \left(\frac{\sigma_{sf}}{z}\right)^4 - \frac{\sigma_{sf}^4}{3\Delta(0.61\Delta + z)^3}\right\} \quad (1)$$

where the subscripts s and f stand for graphite carbon and the other particles, respectively, z is the distance of particle f from the adsorbing surface, $\Delta = 0.335$ nm is the separation between the graphene sheets, $\rho_s = 114$ nm^{-3} is the number density of the carbon atoms in the graphite wall, $\sigma_{ss} = 0.34$ nm and $\varepsilon_{ss} = 0.2328$ kJ/mol are the Lennard-Jones (LJ) interaction parameters of graphite carbon (see ref 10), and the LJ interaction parameters between unlike particles are obtained by the geometric mean combination rule.

It is worth noting that the Steele 10−4−3 wall potential arises from the integration of the LJ 12−6 interaction with the graphene sheet structure in 3 dimensions, which yields the last term of eq 1. Therefore, the Steele 10−4−3 potential is also a type of short-range interaction. The effective cutoff distance of the Steele 10−4−3 potential is about 5.8 nm, where the error from the Steele 10−4−3 potential is roughly equal to that of LJ 12−6 potential at a cutoff distance of 1.2 nm (the cutoff distance of 1.2 nm is used for the other LJ interactions). In the present work, a higher value of 10 nm is employed. As an example, we plot in Figure 1b the Steele 10−4−3 wall interaction with a sulfur atom on the PSS.

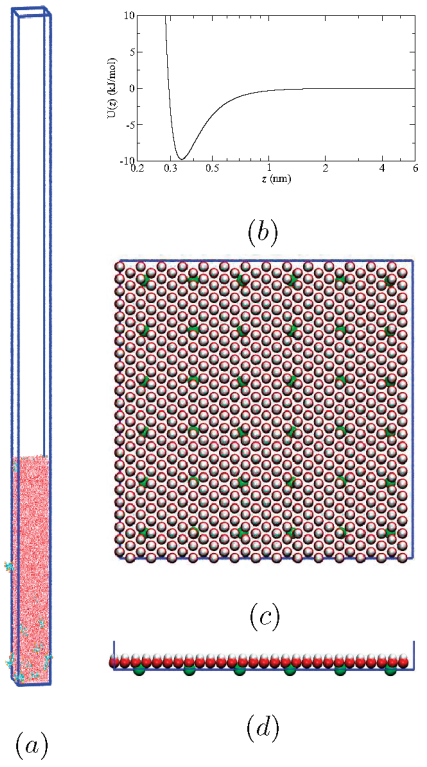

Figure 1. Snapshot of our simulated system with hydrophilic surface and the surface charge density of 0.164 C/m^2. (a) The overall system size is 5.964 × 5.9027 × 87 nm^3 ($X \times Y \times Z$). See the text for more details. Plotted in panel b is the Steele 10−4−3 wall interaction of sulfur atoms on PSS. (c) Top view and (d) side view of the adsorbing surface, where the surface hydroxyl oxygens (hydrogens) are in red (white) and the surface charges are in green. Panels a, c, and d were plotted using VMD.[18]

To model the hydrophilic substrate, we follow the method used in ref 22. Polar hydroxyl groups (−OH) are built on top of every second carbon which is implicitly located on the hydrophobic adsorbing surface modeled via the Steele 10−4−3 potential. See Figure 1c,d for a graphical scheme, where the hydroxyl oxygens and hydrogens are marked in red and white, respectively. On the basis of this approach, a number density of the hydroxyl groups of 19.1 nm^{-2} is generated. The C−O and O−H bond length is 0.136 and 0.095 nm, respectively, corresponding to the parameters of alcohol in the OPLS-AA force field.[23] All the hydroxyl oxygens and hydrogens are distributed vertically on top of the adsorbing surface and fixed at their initial positions throughout the simulation runs. The partial charge of the hydroxyl hydrogen, 0.408 e, is taken from ref 22, while −0.408 e has been chosen for the hydroxyl oxygen to neutralize the hydroxyl group. Note that in ref 22 the COH group rather than the −OH was chosen to be neutral, where C stands for the carbon atoms which are explicitly present on the topmost graphene sheet in their work. The surface is considered hydrophobic when no polar OH groups are present.

To build the charged surface, some dummy particles are fixed uniformly on the top of the substrate, i.e., $z = 0$. Each of the dummy particles carries one monovalent charge and has neither LJ interaction nor mass. In Figure 1c,d, the surface charges are marked in green. In the present work, the surface charge density, σ_s, is varied from 0 to 0.073 to 0.164 C/m^2, which correspond to 0, 16, and 36 unit surface charges, respectively. These surface charge densities lie within the experimentally accessed range reported in refs 11 and 12. To neutralize the surface charges, Cl^- counterions are added, which are randomly distributed in the region $z \in (0,29)$ nm at the beginning of the simulation.

B. PSSNa Solution. In the present work, a PSS monomer concentration of 0.4 M is employed due to the limitation of the system size investigated. Each system consists of 21 PSS chains with DP = 12 and 252 Na^+ counterions. Note that the negligible influence of PE DP on its adsorption has been observed by a CG-level work[14] and a work based on nonlocal density functional theory.[24] Our test demonstrate that the degree of polymerization DP in the range considered here (DP = 12 vs DP = 6) has little influence on the adsorption of PSS sulfonate sulfur and water oxygen, independently of the hydrophobicity or hydrophilicity of the surface (see Figure S1 of the Supporting Information). Considering the fact that the persistence length of PSS is about 1.4 nm[25] and that the contour length of PSS at DP = 12 is about 3.5 nm, the PSS chains of DP = 12 behave rodlike. The overall number of charges resulting from the PSS, 252, is more than 4 times larger[10,14] than that of the surface charges. Being a strong polyelectrolyte, every monomer of PSS is charged. The system size is chosen to be 5.964 × 5.9027 × 29.0 nm^3 in $X \times Y \times Z$ dimensions. A hydrophobic neutral wall is added at $z = 29$ nm to avoid the escape of the particles. In order to determine the number of water molecules to be added, an additional simulation of a homogeneous bulk PSSNa solution with the same number of PSSNa (see system R.0 in Table 1 and ref 26 for the simulation parameters) has been performed in the NPT ensemble. It turned out that to obtain the average volume of 1020.9 nm^3 32 760 water molecules had to be added, resulting in a system density of 1044 kg/m^3.

All initial configurations were built using the package Packmol.[27] To speed up the adsorption kinetics, the PSS chains are initially distributed in the region of $z \leq 14.5$ nm, which is much bigger than the effective cutoff distance of the Steele 10−4−3 wall potential of about 5.8 nm. No salt ions are included in any of the investigated systems.

C. Simulation Details. Classical molecular dynamics simulations are performed using the package GROMACS 4.0.7.[28] Because of the ability to reproduce the hydration behavior and the dielectric constant of water,[29,30] the SPC/E water model[31] has been chosen with a geometry constrained using the SETTLE algorithm.[32] The interaction parameters of PSS, based on the OPLS-AA force field,[23] are reported elsewhere.[26] The potential energy in the OPLS-AA force field has contributions from bond length, bond angle, proper dihedral, improper dihedral (torsion potential), LJ, and Coulomb interactions.

In all the simulations, 2D periodic boundary condition is applied in the XY plane. Neighbor searching is performed up to 1.2 nm and updated every 10 time steps. LJ interactions and forces are cut off at 1.2 nm, and long-range dispersion corrections to potential energy and pressure are applied.

The initial configurations are relaxed by energy minimization using the steepest descent algorithm, followed by a simulation in the NVE ensemble for the duration of 1 ps to further reduce possible overlapping. Subsequently, the temperature is scaled via the Nose-Hoover thermostat (reference temperature $T = 298$ K, characteristic time $\tau = 0.5$ ps), thus realizing a NVT ensemble. The systems are equilibrated for 100 ps. In this phase, the electrostatic interaction is truncated at a cutoff distance of 1.2 nm, and an integration time step of 1 fs is employed.

In the following stages, the particle mesh Eward (PME) method[33,34] is used to perform the electrostatic interaction calculation with a direct space cutoff of 1.2 nm and a Fourier

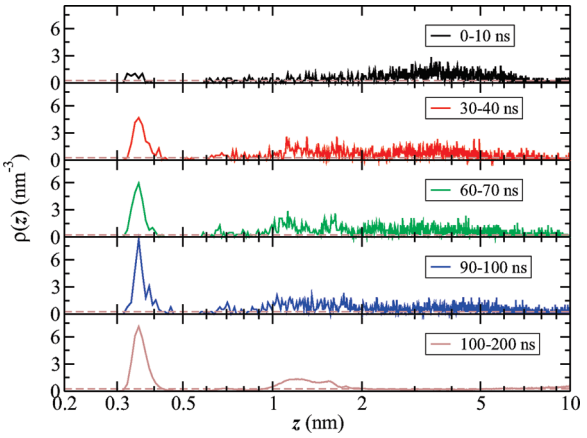

Figure 2. Adsorption process of PSS in system H.1, which is described by the number density profile of the sulfur atoms of the PSS in difference periods. The horizontal dash lines represent the average density of 0.25 nm^{-3}. The smaller fluctuations in the data of 100−200 ns is due to the bigger amount of statistical samples.

grid spacing of 0.12 nm The reciprocal summation of the Ewald formula is performed in 3D, but a dipolar correction term[35] is used to produce a pseudo-2D summation. Furthermore, to reduce the remaining artifacts from the unwanted third dimension, an empty region of z_{void} = 58 nm is added in the Z direction, which results in an overall length in Z dimension of 87 nm, as shown in Figure 1a.

To speed up the simulations, a larger integration time step is needed. To that end, the following procedure is employed: first, the systems are simulated for a duration of 100 ps using the time step of 1 fs, and then another run of 100 ps is performed with a time step of 2 fs by constraining the colavent bonds involving hydrogen atoms. Eventually, a time step of 2.5 fs is employed, and all covalent bonds lengths are constrained using the LINCS algorithm.[36]

The last stage, namely, the production run is performed for a total duration of 200 ns. During the first 100 ns configurations are stored every 1 ns to monitor the adsorption kinetics of PSS. In the subsequent 100 ns, configurations are stored every 10 ps for the analysis of the equilibrium structures. Because of the large number of atoms (about 10^5) in the system, these simulations are very time-consuming, and required about 30 000 CPU hours for each simulation run.

In order to make a comparative analysis, three additional systems (named P.0, H.0, and R.0) are prepared as reference systems (see Table 1 for their compositions). System P.0 (H.0) is similar to system P.1 (H.1) which consists only of water and the wall in order to study the adsorption of water. System R.0 consists only of a PSSNa aqueous solution, without a wall, in order to investigate properties, like the dielectric constant of water, in the bulk.

III. RESULTS AND DISCUSSION

Before starting measuring equilibrium structures, the PSS adsorption process has to be monitored to check for its completion. As an indicator for the adsorption, the number density $\rho(z)$ of sulfur atoms of PSS is monitored as a function of the distance z from the adsorbing substrate. In Figure 2, the results obtained in system H.1 are presented. A qualitatively similar behavior in the adsorption kinetics is found in every other system. Figure 2 clearly shows that the adsorption process can be divided into two stages. (a) In the first one, the PSS chains move toward the adsorbing surface rapidly. This stage is approximately completed in less than 30 ns, causing the formation of two condensed regions at z < 0.5 nm and $z \approx 1-7$ nm. Note that the initial structure, in our cases $z \leq$ 14.5 nm, will most likely affect the adsorption kinetics; however, it will not influence the statics, which is all that we need in the present work. (b) In the subsequent stage, the adsorbed PSS sulfurs rearrange their positions. The adsorption layer at z < 0.5 nm becomes more and more pronounced until it becomes stable. This stage is so slow that the density profile shows some tiny changes even after the duration of 100 ns, as indicated by the different height of the first peak at about z = 0.35 nm.

In a CG-level simulation with structureless solvents explicitly expressed, Reddy and Yethiraj[9] have also claimed the presence of two stages for polyion adsorption: a fast adsorption of polyions followed by a much slower one. Nevertheless, some differences are observed by comparing the CG-level work with the present AA-level one. (a) The first stage was claimed to be caused by the electrostatic attraction between the adsorbing surface and the polyions in ref 9. In the present work, however, we find that such electrostatic attraction is not necessarily required for the PSS adsorption. For instance, a PSS adsorption layer is observed in system H.1 where no Coulomb interaction exists for the adsorbing surface. (b) In ref 9, only under sufficiently poor solvent condition was the second stage observed, where a phase separation between a polyion-rich and a polyion-poor phase occurred, and the polyion aggregates diffused toward the adsorbing surface. In the present work, such phase separation was not observed in the bulk region in any of the investigated systems. This difference may be attributed to the affinity between PE and solvent: in this work, water is not such a poor solvent as that used in ref 9. Such a good affinity between PSS and water probably originates from the polar sulfonate groups preference of pointing away from the PSS backbone due to steric and Coulomb repulsion between neighboring PSS monomers (see, e.g., Figure 5b,c). The presence of the sulfonate groups therefore hinders the hydrophobic effect originating from the PSS backbone.

Because of the slow kinetics of the PSS adsorption, we need to estimate the dependence of our measurements on the initial structure. Systems P.1−3 and H.1−3 have therefore been run for three times using independent initial structures, which were generated with different random seeds in the package Packmol. The average values and the standard deviations of some calculated observables are listed in Table S1 of the Supporting Information. A dependence on the initial structures is observed, but is quite weak, thus confirming the reliability of our results based on these three runs. And in the following sections, all the data reported have been averaged over these three runs for each system, unless otherwise stated.

A. PSS Adsorption. To better compare the adsorption of PSS (and also of/for water) on the hydrophilic surface with that on the hydrophobic surface, we followed the approach applied in ref 37, where the origin of the Z-axis is located at the position of the hydroxyl oxygens in systems P.0−3. This is acceptable by considering the fact that the surface hydroxyl groups in systems P.0−3 are fixed throughout the simulations. Therefore, in what follows, all the coordinates in Z dimension in systems P.0−3 have been decreased by 0.136 nm.

To study the adsorption of the PSS sulfonate groups, we calculated the number density profile $\rho(z)$ of the PSS sulfur atoms. It is necessary to note that in the present work, the term "sulfonate group" stands for the group of $[CSO_3]^-$, which has an

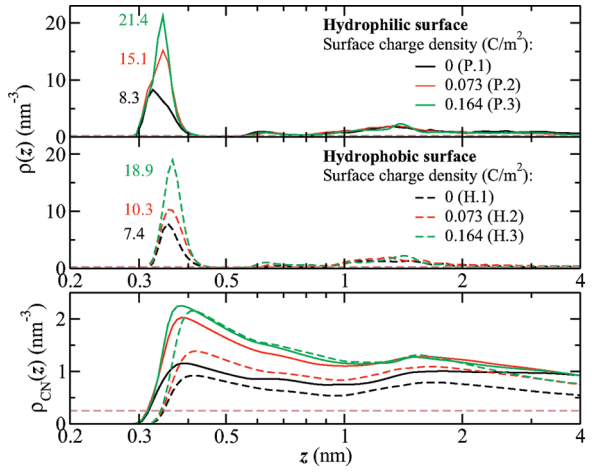

Figure 3. Number density profile of sulfonate sulfur of PSS in systems with (top) hydrophilic and (middle) hydrophobic adsorbing surface. The number density values at the first peak positions are given in the corresponding color. (bottom) The corresponding density profiles of cumulative numbers (eq 2) of sulfur atoms on PSS are plotted. The horizontal dash lines represent the average density of 0.25 nm^{-3}.

overall charge of −1 e and its geometric center is located close to the position of the sulfur atom.[26] In the following calculations of density and related properties, the width of the bin used to sample observables is chosen to be 0.01 nm. The density profiles calculated in systems involving hydrophilic or hydrophobic surfaces are reported in Figure 3. It is shown that in all investigated systems the first adsorption layer occurs in the region up to about 0.5 nm away from the surface. Therefore, the region of the first adsorption layer of PSS sulfonate is defined to be $z \leq 0.5$ nm in the following.

The effect of the surface charge density is demonstrated by the increase in height of the first adsorption peak. By increasing the surface charge density from 0 to 0.073 to 0.164 C/m^2, the peak density in the first adsorption layer increases from 8.3 (P.1) to 15.1 (P.2) to 21.4 (P.3) nm^{-3} in systems with hydrophilic surface. Correspondingly, the increase occurs also in systems with hydrophobic surfaces, but smaller density values are obtained, namely, 7.4 (H.1), 10.3 (H.2) and 18.9 (H.3) nm^{-3}. It is thus concluded that the presence of the surface charges increases the adsorption of PSS sulfonate groups in the first adsorption layer at given hydrophilic (or hydrophobic) surface.

On the other hand, by comparing the data in the systems with a neutral surface, i.e., P.1 vs H.1, the presence of the hydrophilic surface groups is also found to play a role in promoting the adsorption of PSS in the first adsorption layer, which suggests that PSS behaves as a hydrophilic PE with the hydrophobic nature of the PSS backbones screened by the outward extending sulfonate groups. Note that even system H.1 is capable of forming a PSS adsorption layer due to the attractive force of the Steele 10−4−3 potential (see also Figure 1b). For small surface charge densities like σ_s = 0.073 C/m^2 (P.2 vs H.2), the strong effect of the surface hydroxyl groups, $\Delta\rho$ = 4.8 nm^{-3}, suggests that the coexistence of surface hydroxyl groups and surface charges promotes mutually the PSS adsorption. However, for the largest surface charge density of σ_s = 0.164 C/m^2 (P.3 vs H.3), only a weak influence of the surface hydroxyl groups (i.e., $\Delta\rho$ = 2.5 nm^{-3}) is observed, which is related to the saturation of PSS adsorption. This will be discussed later.

It is also shown in Figure 3 that the first adsorption peak is located at $z \approx 0.35$ nm from the adsorbing surface, which approximately corresponds to the position of the strongest attractive interaction of the Steele 10−4−3 wall potential, as shown in Figure 1b. Moreover, the fluctuations of the density profiles in Figure 3a,b extend up to about 2 nm away from the adsorbing surface, which is also consistent with the Steele 10−4−3 wall potential. These findings indicate that the Steele 10−4−3 wall potential plays a significant role in the adsorption of PSS sulfonate.

It is worth noting that some previous Monte Carlo works[38,39] have shown that short-range attractive forces of nonelectrostatic origin are needed to produce stable PEMs, where the CG-level PEs are deposited onto charged sphere and rod substrates. Regardless of the difference between PEM and PSS monolayers, our calculation in system H.1 shows that the exclusive presence of the Steele 10−4−3 wall potential is strong enough to form a stable PSS adsorption layer. A further investigation on the substrate effect on poly(styrenesulfonate)/poly(diallyldimethylammonium) (PSS/PDADMA) bilayer formation is underway and is expected to provide better understanding on the role of short-range nonelectrostatic interaction.

To further compare the adsorption ability of the different adsorbing surfaces, the cumulative number density, $\rho_{CN}(z)$, is calculated according to[37]

$$\rho_{CN}(z) = \frac{\int_0^z \rho(r) S \, dr}{\int_0^z S \, dr} \qquad (2)$$

where S = 35.2037 nm^2 is the surface area of the simulation box in the XY plane. In comparison with the number density in certain distance bin $\rho(z)_{r\in[z-dr/2,z+dr/2)}$, the cumulative number density $\rho_{CN}(z)$ describes the average adsorption ability in the distance range of $r \in [0, z]$ nm. The obtained results for the sulfur atoms on PSS are reported in Figure 3. First of all, it is worth to note that even though both the presences of the surface hydroxyl groups and the surface charges have the capability of promoting the adsorption of PSS as previously discussed, the adsorption has some limitation (i.e., saturation) due to the steric and electrostatic repulsion between the adsorbed PSS monomers.

As demonstrated in Figure 3c, in systems with neutral surfaces (P.1 and H.1), the strong influence of the hydrophilic hydroxyl groups is indicated by the evident difference of the adsorption of PSS sulfonate groups throughout the investigated distance range. On the other hand, in systems with σ_s = 0.164 C/m^2 (P.3 and H.3), the almost overlapping curves of PSS sulfonate adsorption suggest a negligible effect of the hydrophilic hydroxyl groups on the adsorption and probably the saturation of the adsorption. Note that the standard deviation is about 5% of the corresponding average value (see Table S1 of the Supporting Information).

Regarding the effect of the surface charges on PSS adsorption at hydrophilic (or hydrophobic) surface, one should introduce different regions according to the distance from the adsorbing surface. In the short distance range of z < 1.5 nm, the adsorption ability depends roughly monotonically on the surface charge density. In systems with hydrophobic surface (i.e., H.1−3) such relation is evident, while it becomes less clear in systems with hydrophilic surface (namely P.1−3 and in particular in P.2 and P.3). This can be probably attributed to the fact that the coexistence of hydrophilic groups and charges on the surface facilitates the achievement of the saturation of PSS adsorption.

In the longer distance range, however, the influence of the surface charges on PSS adsorption disappears. It can be seen in Figure 3 that all the cumulative number density curves are overlapping if one takes the standard deviations into consideration (the exception of system H.1 might be attributed to the weakest attractive surface interaction). The disappearance of the surface charge influence can be interpreted on the basis of the adsorption of PSS chains (see Figure 5) rather than that of PSS sulfonate groups: the density profiles of the sulfonate sulfurs in the region $z > 1.5$ nm are mainly due to the nonadsorbed PSS chains.

In combination with the previous discussions on the effects of the hydrophilic hydroxyl groups and the charges on the surfaces, it can be concluded that: (i) At low surface charge density both the presences of the polar surface hydroxyl groups and the surface charges promote the adsorption of PSS sulfonate groups. (ii) At the highest surface charge density investigated, σ_s = 0.164 C/m^2, the adsorption of PSS sulfonate groups is approximately saturated. In such case, the adsorption is dominated by the electrostatic attraction originating from the surface charges.

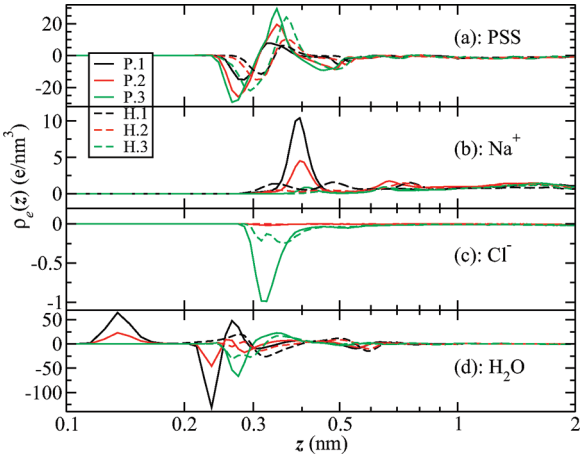

Figure 4. Charge density profiles of (a) PSS, (b) Na^+, (c) Cl^- (if any), and (d) water as a function of the distance z from the adsorbing surface. See Table 1 for the labels of the systems.

Because of the high number of charges present in the system, it is also interesting to investigate the effect of the surface on the charge distribution. The charge density profiles of the different charged species are presented in Figure 4. The interfacial fluctuations of PSS charge density are shown to extend up to about 1 nm away from the surface. The first negative peaks at $z \approx 0.27-0.31$ nm in Figure 4a are due to the aggregation of the sulfonate oxygens, while the first positive peaks at $z \approx 0.33-0.36$ nm come from the aggregation of sulfonate sulfurs. Note that the partial charge of sulfur, oxygen, and carbon chemically bonded to sulfur in the sulfonate is 1.48 e, −0.68 e, and −0.44 e, respectively.[26] This explanation is also supported by the density profiles of sulfonate oxygen and sulfur (see Figure S2 of the Supporting Information). Moreover, it is shown in Figure 4a that in the presence of either hydrophilic hydroxyl groups and/or charges on the surfaces, the layered adsorption of sulfurs and oxygens from the sulfonates is promoted.

Compared with the charge densities of PSS, those of Na^+ and Cl^- are negligible in most of the investigated systems (except those of Na^+ in systems P.1−2) as shown in parts b and c of Figure 4, respectively. This agrees with the statement that with the increase of the PEs adsorbed onto substrate the small ions (for instance, Na^+, Cl^-) are expelled away from the substrate, which has been explained to be the entropy gain originated from the release of the small ions (see, e.g., ref 40). A further detailed study showed that: (a) The presence of the surface hydroxyl groups promotes the adsorption of both Na^+ and Cl^-: the peak in system P.1 (P.2, P.3) is more pronounced than the corresponding one in system H.1 (H.2, H.3). (b) As expected, the positive surface charges expel Na^+ and adsorb Cl^-: the peak positions of Cl^- are about 0.1 nm closer to the adsorbing surface.

The previous discussions have shown that the adsorption of PSS is predominantly located in the region of $z < 2$ nm. To understand such phenomenon, the adsorption of PSS chains, rather than that of PSS sulfonate groups, needs to be investigated. In the present work, if any of the sulfur atoms on certain PSS chain is adsorbed, i.e., it is located at $z \leq 0.5$ nm, such PSS chain is considered to be adsorbed. The average thickness of the layer of adsorbed PSS chains can be obtained using a lattice method.[41] First, the XY plane is partitioned on a lattice with grid size of

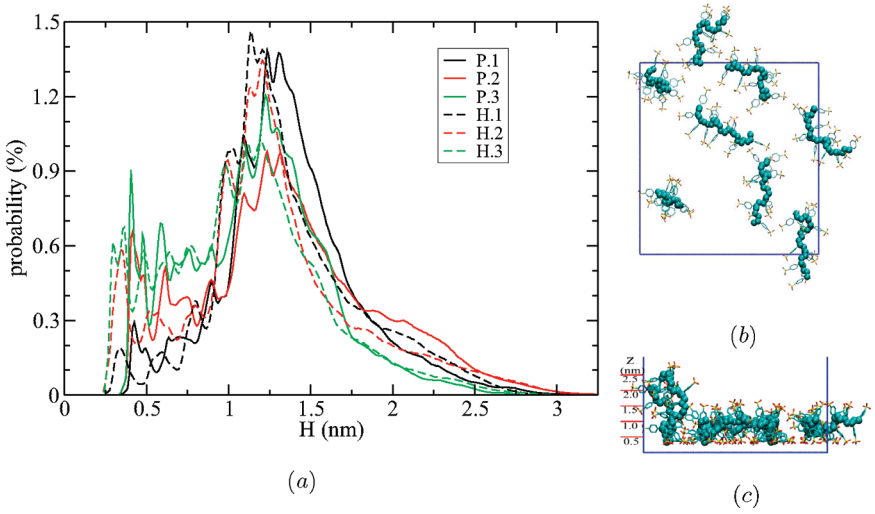

Figure 5. (a) Distribution probability of the layer thickness H of the adsorbed PSS chains. (b) Top view and (c) side view of the adsorbed PSS chains in the last frame of system H.3. The PSS backbones are in blue in the VDW rendering method, and hydrogen atoms and surface charges are not shown for clarity. In panel c, the distance to the adsorbing substrate is labeled in nm.

0.15 nm × 0.15 nm. The value of 0.15 nm is chosen to be approximately equal to the carbon−carbon bond length of 0.153 nm. The thickness of the layer in correspondence of a grid element is then estimated by taking the maximum height of the adsorbed PSS atoms lying within the grid element. Thereby, the distribution of the thickness is obtained by exploring all the lattice elements and throughout the simulation duration. The results are plotted in Figure 5a. From Figure 5a, the following information can be extracted: (a) The dominant contribution to the distribution in the distance range of 1−1.5 nm is attributed to the PSS chains which lay on the *XY* plane with their backbones approximately parallel to the *XY* plane, as shown in Figure 5c. (b) The relatively weaker peak at $z < 0.5$ nm originates also from the laying PSS chains, but in this case these PSS atoms extend toward the *XY* plane away from their backbone. (c) The maximum height of the adsorbed PSS chains is about 3 nm, and this happens when the backbones of the adsorbed PSS chains are standing on top of the adsorbing surface, as shown in Figure 5c.

Experimentally, Block and Helm[7,42] have found that even though the flat PSS adsorption layer dominates, some adsorbed PSS chains dangle into the above PSS solution, where PSS were physisorbed on a solid silica surface. In particular, at the very low NaCl concentration of 1 mM, the adsorbed PSS chains (DP ≈ 1910) can dangle into the PSS solution up to about 120 nm, which is about 30% of the contour length.[42] In the present work, the height of 3 nm represents ≈86% of the PSS contour length, which is much larger than the experimental value of 30%[42] and is expected to result from the rodlike behavior of PSS with DP = 12. Moreover, in a CG-level work,[9] the partially standing polyion chains (up to ≈5 out of DP = 10) was also observed under good solvent condition (see Figure 1 of ref 9). Note that in ref 9 the polyion chain was very flexible due to the lack of bond angle and dihedral interactions.

It is also worth pointing out that the positions of the two peaks in Figure 5a (namely, $z < 0.5$ nm and $z \approx 1-1.5$ nm) are approximately consistent with those of the two peaks as shown in Figure 3. When the surface charge density increases, the increasing distribution probability in the region of $z < 0.5$ nm coexists with the decrease of that in the subsequent region, which probably suggests that some PSS sulfonate groups rotate from pointing toward the above solution to extending toward the adsorbing substrate.

The average thickness of the PSS adsorption layer computed from the thickness distribution resulted to be 1.4 ± 0.4 (P.1), 1.4 ± 0.5 (P.2), 1.2 ± 0.4 (P.3), 1.3 ± 0.4 (H.1), 1.3 ± 0.5 (H.2), and 1.1 ± 0.5 (H.3), respectively. These values are indistinguishable within the error bars, and therefore, unlike the case of the CG-level work,[14] the relation between the surface charge density and the average thickness of PE adsorption layer cannot be established here.

By following our definition that one PSS chain is considered to be adsorbed if at least one of its sulfur atoms is located at $z \leq 0.5$ nm, the surface charge overcompensation and the surface coverage[11] can be calculated (see Table 2 for the obtained results). For all systems, we find surface charge overcompensation in the range of 2.1−4.9 PSS monomers per surface charge. The surface charge overcompensation ratio of 2.1 (P.3)/2.4 (H.3) at $\sigma_s = 0.16$ C/m^2 in the present work agrees well with the experimental data of ∼2.3[11] at the same σ_s, and a lower surface charge density yields a higher surface charge overcompensation (see also Figure 10 in ref 11). Our computed surface coverage of Γ = 2.1 (P.3)/2.5 (H.3) PSS monomers per nm^2 of the surface area at $\sigma_s = 0.16$ C/m^2 is also consistent with the experimental finding in ref 11 where $\Gamma \approx 2.2$ was reported at the same σ_s, and with the decrease of the surface charge density, the surface coverage is also decreasing (see also Figure 12 in ref 11). (In ref 42 the authors claimed a low surface coverage ($\Gamma \approx 0.7$) of PSS adsorption on a silica substrate. It might be probably ascribed to a very low surface charge density, or even a neutral surface, which was unfortunately not mentioned in ref 42.)

Table 2. Calculated Values of Some Observables

	charge overcompensation				
system	Q_s[a]	$\langle\lvert Q_{PSS}\rvert\rangle$[b]	$\langle\lvert Q_{PSS}\rvert\rangle/Q_s$[c]	Γ[d]	ε[e]
P.1	0	61		1.7	29
P.2	16	78	4.9	2.2	24
P.3	36	75	2.1	2.1	21
H.1	0	56		1.6	37
H.2	16	71	4.4	2.0	29
H.3	36	88	2.4	2.5	19

[a] Number of surface charges (in unit of e). [b] $\langle\lvert Q_{PSS}\rvert\rangle$/e is average number of monomers on those adsorbed PSS chains (a PSS chain is considered to be adsorbed if at least one of its sulfur atoms is located in the region of $z \leq 0.5$ nm). The maximum standard deviation is ∼20% of the corresponding average value. [c] From Figure 10 of ref 11 ∼2.3 PSS monomers per surface charge of DODAB monolayer was found at $\sigma_s = 0.16$ C/nm^2, and a lower surface charge density yields a higher surface charge overcompensation. [d] Surface coverage $\Gamma = (\langle\lvert Q_{PSS}\rvert\rangle/e)/S$ (where $S = 35.2037$ nm^2 is the area of the adsorbing surface). In Figure 12 of ref 11, $\Gamma \approx 2.2$ at $\sigma_s = 0.16$ C/nm^2, and a lower surface charge density induces a lower surface coverage. [e] Dielectric constant of water obtained up to $z = 0.8$ nm (see Figure 6). $\varepsilon = 63 \pm 1$ in bulk PSS solution of system R.0.

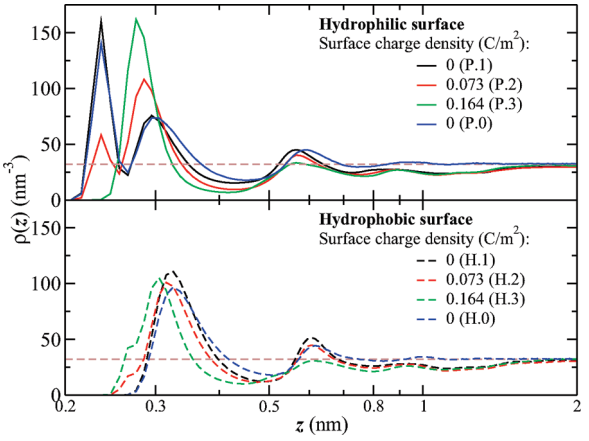

Figure 6. Number density profiles of water oxygens in systems with (top) hydrophilic and (bottom) hydrophobic surface as a function of the distance z from the adsorbing surface. The horizontal dash lines represent the average density of 32.1 nm^{-3}.

B. Water Adsorption. Similar to the previous study on PSS adsorption, the number density profiles of water oxygens along the adsorbing surface normal are calculated and presented in Figure 6. It is seen that the interfacial fluctuations substantially ceased in the region of $z > 2$ nm in all the investigated systems. The water oxygen density profiles are characterized by two peaks, which are located at about 0.28−0.34 and 0.6 nm from the adsorbing surface. It is noteworthy that the aggregation of the first water oxygen layer is slightly closer to the adsorbing surface than that of the first PSS sulfur peak ($z \approx 0.35$ nm), which indicates a sandwich-like distribution of

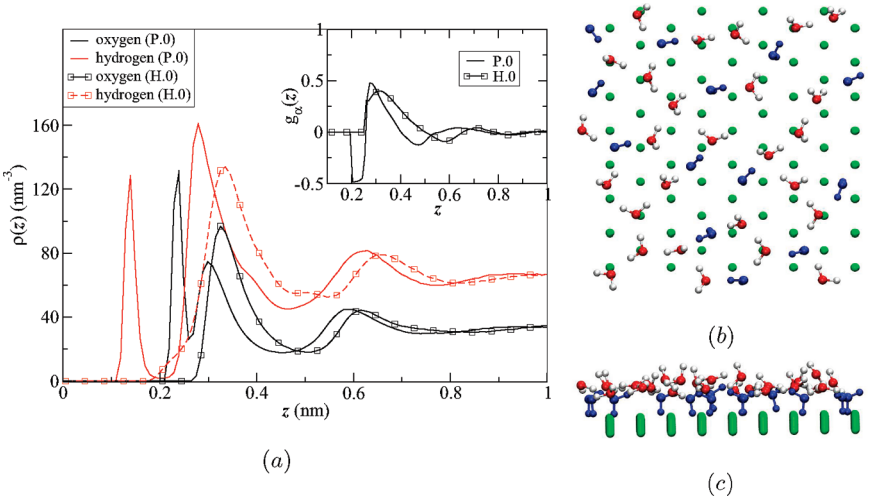

Figure 7. Layer structures of waters close to the adsorbing surface. In panel (a), the number density profiles of water oxygen and hydrogen in systems P.0 and H.0 are given. In the inset, $g_\alpha = -0.5$, 1, and 0 represents vertical, parallel, and random orientation, respectively, between the water plane and the *XY* plane (see eq 3). (b) Top view and (c) side view of the waters in the first layer (in blue, $z \leq 0.26$ nm in oxygen coordinate) and the second layer (oxygen/hydrogen in red/white, respectively, $z \in (0.26, 0.42]$ nm in oxygen coordinate) in system P.0. Water is drawn in the CPK rendering method, while the licorice method for hydroxyl groups (in green). In panels b and c, only a fraction of the adsorbing surface with the area of 2×2 nm^2 ($X \times Y$) is plotted.

water molecules between the substrate and the first PSS aggregation layer. This sandwich-like layer structure can be probably attributed to the presence of the hydrogen bonding (HB) between sulfonate and water, and (or) surface hydroxyl groups and water, as discussed later.

Note that even though the hydrophobic neutral wall is exclusively employed for the surface interaction in systems H.0−1, the adsorption of water is also seen in close contact with the adsorbing surface, which is similar as that in refs 43−45. This is due to the attractive interaction of the Steele 10−4−3 potential (see Figure 1b). Another interesting finding is that, in the case of neutral surface, the water structures have little dependence on whether there is PSS adsorbed (system P.1) or not (system P.0) at a given hydrophilic surface. This also holds in systems with hydrophobic surfaces (H.1 vs H.0).

Moreover, as shown in Figure 6a, there is an additional peak at $z \approx 0.24$ nm in systems P.0−2. To understand the orientations of the water molecules located at about 0.24 nm, the density profiles of water oxygens and hydrogens in system P.0 are calculated and plotted in Figure 7a. The first peak of the water hydrogens is located at 0.135 nm, to be compared to that of the water oxygens at 0.235 nm. The distance difference between them agrees well with the bond length of O−H in SPC/E water model of 0.1 nm. Moreover, the number density of the water hydrogens at 0.135 nm is approximately equal to that of the water oxygens at 0.235 nm. The arrangements of the water molecules in both the first layer ($z \leq 0.26$ nm) and the second layer ($z \in (0.26,0.42]$ nm) are shown in panels b and c of Figure 7. The hydrogen-down-oriented water molecules[44,45] are highlighted in blue, where one of the water hydrogens is located right below the water oxygen. Note that in systems P.3 and H.0−3 such hydrogen-down orientation disappears, as indicated by the overlapping positions of the first peaks of water oxygens and hydrogens in system H.0, as shown in Figure 7a (a more detailed calculation of the number density profiles of water oxygens and water hydrogens of systems P.1−3 and H.1−3 can be found in Figure S3 of the Supporting Information). Moreover, in the second layer region in system P.1, most water molecules prefer an orientation which is approximately parallel to the XY plane, as shown in Figure 7b,c.

On the other hand, in system H.0, even though both of the first peaks of water oxygens and hydrogens are located at about z = 0.32 nm, the value of water hydrogen number density at z = 0.32 nm (≈ 133 nm^{-3}) is less than twice that of water oxygen (≈ 95 nm^{-3}). Comparably, in the distance range up to about z = 0.28 nm, the former is more than 2 times larger than the latter. This finding indicates a weak both-hydrogens-down orientation in such region in system H.0, that is, both of the two water hydrogens, rather than the water oxygen, prefer to point toward the adsorbing surface. This water orientation probably coexits with a tilted hydrogen-down water orientation.

To characterize quantitatively the orientation of water molecules, we computed the second rank orientational order parameter

$$g_\alpha(z) = \frac{1}{N(z)} \sum \left[\frac{1}{2} (3 \cos^2(\alpha(z)) - 1) \right] \qquad (3)$$

where α is the angle between the normal of the water plane and that of the *XY* plane and z is the distance of water oxygen from the adsorbing surface. The obtained results of system P.0 and H.0 are shown in the inset of Figure 7a. The vertical orientation, $g_\alpha \approx -0.5$, in the region of $z \in (0.2, 0.25)$ nm in system P.0 can be reasonably ascribed to the hydrogen-down orientation, which is absent in system H.0. On the other hand, the maximum of $g_\alpha \approx 0.5$ supports a weak parallel orientation of water molecules to the *XY* plane in the region $z \in (0.26, 0.32)$ nm in both systems P.0 and H.0.

To understand the previously discussed water orientations in the region very close to the surface, one needs to investigate HB. As shown in Figure 7b, in systems with hydrophilic surface, the waters in close contact with the surface are generally located above the center of the triangular structure formed by the hydroxyl groups, and thus HB is expected between the hydroxyl groups and the water molecules. On the basis of the criteria of donor−acceptor distance of $r_{HB} \leq 0.35$ nm and acceptor−donor hydrogen angle of $\alpha_{HB} \leq 30°$, the average HB number is calculated. The obtained values are plotted in Figure 8. Considering that the overall number of the hydroxyl groups is 672, more than half of the hydroxyl groups are involved in HB formation with water. With the increase of PSS

dx.doi.org/10.1021/ma1026109 |*Macromolecules* 2011, 44, 1707–1718

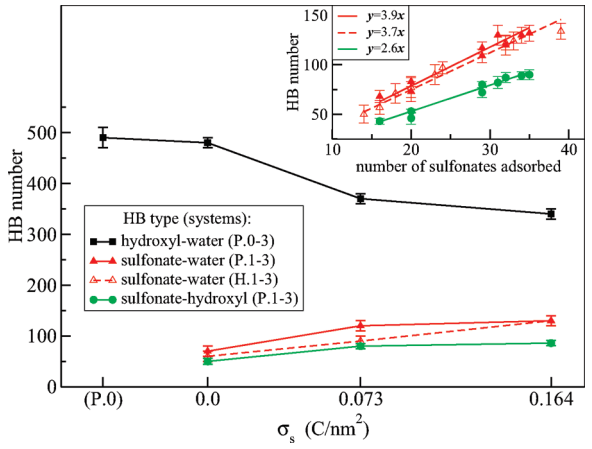

Figure 8. Hydrogen-bonding numbers of hydroxyl−water, sulfonate−water, and hydroxyl−sulfonate, where sulfonate represents those located in the first adsorption layer ($z \leq 0.5$ nm in sulfur coordinate). In the inset the relation between the number of the adsorbed sulfonates and the number of involved HBs is plotted, where data from parallel runs are not averaged, and the standard deviations of the fitted slopes are 0.1.

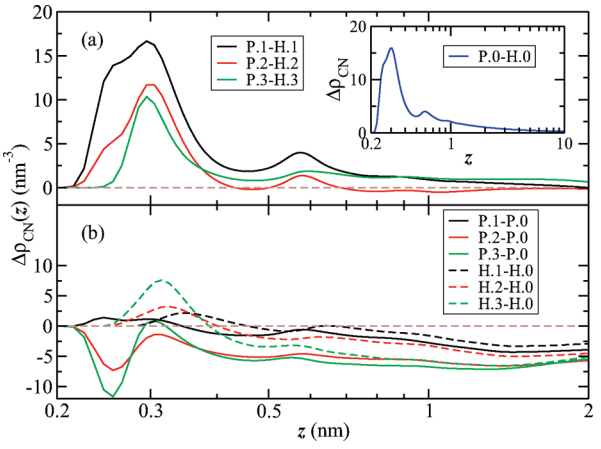

Figure 9. Profiles of the scaled cumulative number density (see eq 4) of water oxygens as a function of the distance z from the adsorbing surface. In panel a, the effect of the surface hydroxyl groups is plotted. In panel b, the influence of the PSS on water adsorption is shown.

adsorption from system P.1 to P.2 to P.3, the HBs between water and the hydroxyl groups are destroyed. Moreover, an approximately equal amounts of hydroxyl−water HB are obtained in systems P.1 and P.0, which is similar as Figure 6.

The calculation of the HB number between the adsorbed sulfonate groups (i.e., $z \leq 0.5$ nm in sulfur coordinate) and the waters is also performed, where the sulfur atoms are serving as HB acceptors, as reported in Figure 8. Here, similar criteria to those employed when computing hydroxyl−water HB calculations are used, except for the donor−acceptor distance, which is in this case $r_{HB} \leq 0.47$ nm, namely, the distance of the first minimum on the donor−acceptor radial distribution function obtained from system R.0. As expected, the adsorption of PSS increases the formation of the sulfonate−water HBs in the calculated region. In combination with the calculations of the hydroxyl water and the sulfonate water HBs, it is indicated that with the increase of PSS adsorption in systems with hydrophilic surface, the overall number of HBs involving water is decreasing in the region close to the surface, while the opposite happens in systems with hydrophobic surface.

Additionally, we calculated the HBs between the hydroxyl groups and the sulfonate groups for the systems with hydrophilic surfaces. The average HB numbers obtained using the same criteria as for sulfonate−water HB are reported in Figure 8.

In the inset of Figure 8, the relation between the number of the adsorbed sulfonate groups and the HB number involving them is reported. It shows that, regardless of the hydrophilicity or hydrophobicity of the surfaces, a linear relation is approximately followed. The sulfonate−water HB number per adsorbed sulfonate group shows little dependence on the hydrophilic or hydrophobic surface feature ($y = 3.9x$ vs $y = 3.7x$ with an error on the slope of 0.1). It is noteworthy that the average number of the sulfonate−water HBs per sulfonate group in bulk PSSNa solution in system R.0 is 4.7 ± 0.1, indicating a more compact structure accompanied by less bounded waters in the PSS adsorption layer than in the PSS bulk solution. The slope of the sulfonate−hydroxyl HBs (2.6) is smaller than those of the sulfonate−water HBs. This is due to the lower dimension (i.e., 2D) distribution of the surface hydroxyl groups and a large distance of 0.246 nm between the nearest hydroxyl oxygens.

To investigate the water adsorption originated from the different surface features (i.e., presence of surface hydroxyl groups and surface charges), the scaled cumulative number density of water oxygens is calculated according to

$$\Delta\rho_{CN}(z) = \rho_{CN}(z) - \rho^0_{CN}(z) \qquad (4)$$

where ρ^0_{CN} is the reference cumulative number density of water oxygens for each comparison.

In Figure 9a, the influence of the surface hydroxyl groups is shown. First of all, the main consequence of the hydrophilic nature of the hydroxyl groups can be seen by comparing systems P.0 and H.0, as shown in the inset: more waters are adsorbed in system P.0 than that in system H.0 ($\Delta\rho_{CN} = \rho^{P.0}_{CN} - \rho^{H.0}_{CN} > 0$) in the region up to at least $z = 10$ nm.[45] Furthermore, the effect of the surface hydroxyl groups is becoming weaker and weaker with increasing surface charge density, as indicated by the decrease of $\Delta\rho_{CN}$ in the short distance range in Figure 9a.

Similarly, panel b shows the dependence of the adsorption of water molecules on that of PSS. The value $\Delta\rho_{CN} < 0$ after the first PSS layer shows that the presence of PSS decreases the adsorption of water with respect to the PSS-free case. This holds for the long distance range, e.g., $z > 1$ nm. Nonetheless, an interesting behavior occurs in the very short distance range of $z < 0.35$ nm: (a) In systems with hydrophobic surface, the adsorption of PSS promotes the adsorption of water in such region: $\Delta\rho^{H.3-H.0}_{CN} > \Delta\rho^{H.2-H.0}_{CN} > \Delta\rho^{H.1-H.0}_{CN} > 0$. (b) While in systems with hydrophilic surface, the neutral surface with PSS adsorbed on top of it (P.1) facilitates the adsorption of the water molecules ($\Delta\rho_{CN} > 0$), the charged surfaces (P.2, P.3) prevent this behavior ($\Delta\rho_{CN} < 0$). This dependence of the water adsorption on the surface features is probably related to the overall number of HBs with water as shown in Figure 8: the increasing overall HB number involving water molecules corresponds to a higher water adsorption.

The charge density of water is also calculated and plotted in Figure 4d. In agreement with the finding reported in ref 45, the surface features perturb the charge profile of water only up to about 1 nm. Such surface fluctuation region is also consistent with the others shown in Figure 4a−c. Considering the partial charges of water oxygen (−0.8476 e) and hydrogen (0.4238 e), the positive and negative peak in Figure 4d originate from the dominating aggregation of water hydrogens and oxygens, respectively.

dx.doi.org/10.1021/ma1026109 |*Macromolecules* 2011, 44, 1707–1718

In systems P.0−2, the previously discussed picture of hydrogen-down orientation is supported by the relative positions of the water hydrogen and oxygen accumulation layers. On the other hand, in systems H.0 and H.1, the charge density peak originated from water hydrogen (oxygen) is located at about 0.28 (0.32) nm, and the strengths of them are approximately equal to each other, supporting the previously discussed picture of weak both-hydrogens-down orientation based in Figure 7a. On the contrary, in systems P.3 (and H.3), the first evident peak occurs with a negative value at $z \approx$ 0.27 nm and is followed by a positive peak at $z \approx 0.34$ nm, which suggests that both of the water hydrogens, rather than the oxygen, prefer to point away from the adsorbing substrate. This kind of both-hydrogens-up orientation is very weakly indicated by the asymmetric and less-pronounced charge densities of these two peaks. Such picture of both-hydrogens-up orientation of water is also supported by the number density of water oxygens and water hydrogens (see Figure S3 of the Supporting Information).

As it has been discussed in our previous work,[26] the static dielectric constant (relative permittivity) of water in the condensed PSS/PDADMA mixtures was calculated to be 9−17, which is consistent with the experimental value of less than 19 in the central region of PSS/PDADMA PEMs. To further investigate the space dependence of the dielectric constant of water, which is significant to the aim of refining our CG-level work with implicit solvent,[16] the dielectric constant of water in the region close to the adsorbing substrate is also calculated here. The dielectric constant ε depends on the total dipole moment $\vec{M} = \sum_{i=1}^{N} \vec{\mu}_i$ and is calculated as[46,47]

$$\varepsilon = 1 + \frac{1}{3Vk_B T\varepsilon_0}(\langle \vec{M}^2 \rangle - \langle \vec{M} \rangle^2) \quad (5)$$

where V is the accessible volume, T is the temperature of the system, ε_0 is the dielectric constant in vacuum, and angular brackets represent the average over time. The dielectric constant of SPC/E water has been previously reported to be 71 ± 6 in the pure water system,[48] and it is here measured to be 63 ± 1 in the 0.4 M PSSNa solution (i.e., system R.0).

To study the effect of the adsorbing substrate on the dielectric constant of water, only those water molecules whose oxygen atoms are located at $z \leq 0.8$ nm (see Figure 6) are considered. The calculated data are listed in Table 2. Regardless of the hydrophilicity or hydrophobicity of the surface, these results show that the adsorption of PSS decreases the dielectric constant of water. The relation roughly follows a monotonic decreasing function. Furthermore, in systems P.3 and H.3, the calculated dielectric constants of water are approximately equal to each other and close to the value of 9−17 obtained in condensed PSS/PDADMA mixtures.[26]

To understand the decrease of the dielectric constant of water, eq 5 is rewritten as

$$\varepsilon = 1 + \frac{\langle \vec{\mu}^2 \rangle}{3k_B T\varepsilon_0} \frac{N}{V} \frac{\langle \vec{M}^2 \rangle - \langle \vec{M} \rangle^2}{N\langle \vec{\mu}^2 \rangle} \quad (6)$$

where $\langle \vec{\mu}^2 \rangle$ is the average unit dipole moment of water molecule, N/V represents the local number density of water in the investigated region, and $(\langle \vec{M}^2 \rangle - \langle \vec{M} \rangle^2)/(N\langle \vec{\mu}^2 \rangle)$ is related to the dipole−dipole correlation.[44,49] The local mass density of water is 763 ± 7 (P.1), 690 ± 20 (P.2), 630 ± 10 (P.3), 750 ± 10 (H.1), 680 ± 10 (H.2), and 621 ± 6 kg/m^3 (H.3). Considering the density of bulk SPC/E waters of ≈1000 kg/m^3 and ε = 71, the relation between the local density and the dielectric constant of water is found to be monotonic but not linear. On the other hand, the waters near the surface are strongly correlated with the surrounding, leading to a reduction of its ability to respond to external potential. A similar finding has been found in our recent work[26] on the condensed PSS/PDADMA mixture.

IV. CONCLUSIONS

We extensively investigated the effects that hydrophilic or hydrophobic surfaces with variable surface charges have on the adsorption behavior of oligomeric (DP = 12) PSS chains using all-atom molecular dynamics simulations. To the best of our knowledge, this is the first work dealing with polyelectrolyte adsorption where both the polyelectrolytes and the solvent are explicitly treated at the all-atom level. Our simulations highlight some features which facilitate the understanding of the equilibrium structures of the adsorbed PSS chains that go beyond the ability of existing experiments and computational works done at the coarse-grained level.

In particular, we found that both the peak positions and the interfacial fluctuations of the sulfonate adsorption profiles are consistent with the short-range interactions originating from the adsorbing substrate (i.e., the Steele 10−4−3 wall potential). The attraction of the Steele 10−4−3 wall potential alone is strong enough to produce a stable PSS adsorption layer. The additional presence of the hydrophilic hydroxyl groups and charges on the surface can further enhance the adsorption of PSS sulfonate. Our results therefore suggest that PSS behaves like a hydrophilic polyelectrolyte. It is only in the case of the highest investigated surface charge density condition, i.e., $\sigma_s = 0.164$ C/m^2, that the adsorption of the sulfonate groups on PSS is dominated by the electrostatic attraction from the oppositely charged surface charges.

In the region close to the adsorbing substrate, the charge densities follow the order of $H_2O \gg$ PSS $\gg Na^+ \gg Cl^-$. The interfacial width of these charge densities extend up to about 1 nm, which is within the region of the adsorption layer of the PSS chains. Two types of conformations of the adsorbed PSS chains are observed. Most of them tend to align parallel to the adsorbing substrate. However, another type of conformation found less frequently consists of PSS chains standing approximately vertically on the surface, which is in qualitative agreement with a previous experimental work, and a CG-level work under good solvent condition.

The calculated surface charge overcompensation and the surface coverage are both in good agreement with the previous experimental data[11] of PSS adsorbed on top of DODAB monolayer. With the increase of the surface charge density, the surface charge overcompensation decreases, while the surface coverage increases.

Between the first adsorption layer of PSS sulfonate and the adsorbing substrate, a water-rich region is found in all investigated systems. The orientation of the water molecules in this region shows a strong dependence on the surface features. In case of a hydrophilic surface, we find a strong one-arm hydrogen-down orientation of water molecules very close to the neutral surface regardless of the presence of adsorbed PSS chains. With the increase of the surface charge density from 0 to 0.073 to 0.164 C/m^2 (and the concurrent increase of the density of the adsorbed PSS sulfonate groups), this hydrogen-down orientation becomes weaker and disappears in case of the highest surface charge density.

For neutral hydrophobic surfaces both of the two water hydrogens prefer to point toward the adsorbing surface, meaning that the water dipole moment points approximately normal to the surface. Quite on the contrary, for the system with the highest surface charge density, we observe an opposite water orientation,

namely both water hydrogens point weakly upward, meaning also that the dipole moment of the water is now reverted. The switch of the orientation of the surface water probably results from the formation of HBs between these waters and the above adsorbed PSS sulfonate groups and the more favorable electrostatic interaction with the positively charged surface.

Regardless of the hydrophilicity or hydrophobicity of the surface, the HB number involving the adsorbed PSS sulfonate groups increases linearly as a function of the amount of the adsorbed sulfonates. Every adsorbed PSS sulfonate group is able to form about 4 HBs with the surrounding waters (slightly smaller than the value of 4.7 found in bulk PSSNa solution) and 2.6 HBs with the surface hydroxyl groups. When the surface charge density is increased, we observe that the HBs between the waters and the surface hydroxyl groups are increasingly broken.

By measuring the dipole fluctuations of the water molecules close to the surface, we find that the local dielectric constant decreases roughly linearly with the increase of sulfonate adsorption in all the investigated systems. It is noteworthy that in systems with the highest surface charge density investigated here, i.e., $\sigma_s = 0.164$ C/m^2, the calculated dielectric constant of waters is about 20, which shows little dependence on whether the surface is hydrophilic or hydrophobic.

The present work serves as a reference for studying polyelectrolyte bilayers on surfaces. A system consisting of PSS/PDADMA bilayers is presently under investigation.

■ ASSOCIATED CONTENT

Supporting Information. Here we present the effect of the original structures on some observables, the influence of PSS DP (DP = 12 vs DP = 6) on the adsorption of sulfonate sulfurs and water oxygens, the layer structure of sulfonate sulfurs and oxygens on PSS on top of the adsorbing surface, water orientations illustrated by the relative number density profiles of water oxygen and water hydrogens. This material is available free of charge via the Internet at http://pubs.acs.org.

■ AUTHOR INFORMATION

Corresponding Author
*E-mail: holm@icp.uni-stuttgart.de.

■ ACKNOWLEDGMENT

B.Q. and C.H. acknowledge support provided through the DFG via the SPP 1369 under grant HO 1108/17-1. J.J.C. thanks the financial support of Spanish Ministerio de Educación y Ciencia, postdoctoral grant No. EXP2006-0931. We thank the HLRS for providing the necessary computer resources needed to complete this study and Marcello Sega for a critical reading of the manuscript.

■ REFERENCES

(1) Netz, R. R.; Andelman, D. *Phys. Rep.* **2003**, *380*, 1–95.
(2) Claesson, P. M.; Poptoshev, E.; Blomberg, E.; Dedinaite, A. *Adv. Colloid Interface Sci.* **2005**, *114−115*, 173–187.
(3) Dobrynin, A. V.; Rubinstein, M. *Prog. Polym. Sci.* **2005**, *30*, 1049–1118.
(4) Dobrynin, A. V. *Curr. Opin. Colloid Interface Sci.* **2008**, *13*, 376–388.
(5) Schmitt, J.; Decher, G.; Hong, G. *Thin Solid Films* **1992**, *210/211*, 831.
(6) Decher, G. *Science* **1997**, *277*, 1232–1237.
(7) Block, S.; Helm, C. A. *Macromolecules* **2009**, *42*, 6733–6740.
(8) Roiter, Y.; Trotsenko, O.; Tokarev, V.; Minko, S. *J. Am. Chem. Soc.* **2010**, *132*, 13660–13662.
(9) Reddy, G.; Yethiraj, A. *J. Chem. Phys.* **2010**, *132*, 074903.
(10) Chialvo, A. A.; Simonson, J. M. *J. Phys. Chem. C* **2008**, *112*, 19521–19529.
(11) Ahrens, H.; Baltes, H.; Schmitt, J.; Möhwald, H.; Helm, C. A. *Macromolecules* **2001**, *34*, 4504–4512.
(12) Tulpar, A.; Ducker, W. A. *J. Phys. Chem. B* **2004**, *108*, 1667–1676.
(13) Cosgrove, T.; Obey, T. M.; Vincent, B. *J. Colloid Interface Sci.* **1986**, *111*, 409–418.
(14) Carrillo, J.-M. Y.; Dobrynin, A. V. *Langmuir* **2007**, *23*, 2472–2482.
(15) Patel, P. A.; Jeon, J.; Mather, P. T.; Dobrynin, A. V. *Langmuir* **2006**, *22*, 9994–10002.
(16) Cerdà, J. J.; Qiao, B.; Holm, C. *Soft Matter* **2009**, *5*, 4412–4425.
(17) Cerdà, J. J.; Qiao, B.; Holm, C. *Eur. Phys. J. Spec. Top.* **2009**, *177*, 129–148.
(18) Humphrey, W.; Dalke, A.; Schulten, K. *J. Mol. Graphics* **1996**, *14*, 33–38.
(19) Steele, W. A. *J. Phys. Chem.* **1978**, *82*, 817–821.
(20) Cracknell, R. F.; Nicholson, D.; Quirke, N. *Phys. Rev. Lett.* **1995**, *74*, 2463.
(21) Stecki, J. *Langmuir* **1997**, *13*, 597–598.
(22) Horinek, D.; Serr, A.; Geisler, M.; Pirzer, T.; Slotta, U.; Lud, S. Q.; Garrido, J. A.; Scheibel, T.; Hugel, T.; Netz, R. R. *Proc. Natl. Acad. Sci. U.S.A.* **2008**, *105*, 2842–2847.
(23) Jorgensen, W.; Maxwell, D.; Tirado-Rives, J. *J. Am. Chem. Soc.* **1996**, *118*, 11225–11236.
(24) Wang, L.; Liang, H.; Wu, J. *J. Chem. Phys.* **2010**, *133*, 044906–13.
(25) Hoda, N.; Larson, R. G. *Macromolecules* **2009**, *42*, 8851–8863.
(26) Qiao, B.; Cerdà, J. J.; Holm, C. *Macromolecules* **2010**, *43*, 7828–7838.
(27) Martínez, L.; Andrade, R.; Birgin, E. G.; Martínez, J. M. *J. Comput. Chem.* **2009**, *30*, 2157–2164.
(28) Hess, B.; Kutzner, C.; van der Spoel, D.; Lindahl, E. *J. Chem. Theory Comput.* **2008**, *4*, 435–447.
(29) Hess, B.; Holm, C.; van der Vegt, N. *J. Chem. Phys.* **2006**, *124*, 164509.
(30) Hess, B.; van der Vegt, N. F. A. *J. Phys. Chem. B* **2006**, *110*, 17616–17626.
(31) Berendsen, H. J. C.; Grigera, J. R.; Straatsma, T. P. *J. Phys. Chem.* **1987**, *91*, 6269–6271.
(32) Miyamoto, S.; Kollman, P. A. *J. Comput. Chem.* **1992**, *13*, 952–962.
(33) Darden, T.; York, D.; Pedersen, L. *J. Chem. Phys.* **1993**, *98*, 10089–10092.
(34) Essmann, U.; Perera, L.; Berkowitz, M. L.; Darden, T.; Lee, H.; Pedersen, L. *J. Chem. Phys.* **1995**, *103*, 8577.
(35) Yeh, I.-C.; Berkowitz, M. L. *J. Chem. Phys.* **1999**, *111*, 3155–3162.
(36) Hess, B.; Bekker, H.; Berendsen, H. J. C.; Fraaije, J. G. E. M. *J. Comput. Chem.* **1997**, *18*, 1463–1472.
(37) Wang, K.; Zangmeister, R. A.; Levicky, R. *J. Am. Chem. Soc.* **2009**, *131*, 318–326.
(38) Messina, R.; Holm, C.; Kremer, K. *Langmuir* **2003**, *19*, 4473–4482.
(39) Messina, R. *J. Chem. Phys.* **2003**, *119*, 8133–8139.
(40) von Klitzing, R. *Phys. Chem. Chem. Phys.* **2006**, *8*, 5012–5033.
(41) Patel, P.; Jeon, J.; Mather, P.; Dobrynin, A. *Langmuir* **2005**, *21*, 6113–6122.
(42) Block, S.; Helm, C. A. *J. Phys. Chem. B* **2008**, *112*, 9318–9327.
(43) Argyris, D.; Tummala, N. R.; Striolo, A.; Cole, D. R. *J. Phys. Chem. C* **2008**, *112*, 13587–13599.
(44) Argyris, D.; Cole, D. R.; Striolo, A. *Langmuir* **2009**, *25*, 8025–8035.

(45) Argyris, D.; Cole, D. R.; Striolo, A. *J. Phys. Chem. C* **2009**, *113*, 19591–19600.
(46) de Leeuw, S. W.; Perram, J. W.; Smith, E. R. *Proc. R. Soc. London, A* **1980**, *373*, 27–56.
(47) Neumann, M.; Steinhauser, O.; Pawley, G. S. *Mol. Phys.* **1984**, *52*, 97–113.
(48) Kusalik, P. G.; Mandy, M. E.; Svishchev, I. M. *J. Chem. Phys.* **1994**, *100*, 7654–7664.
(49) Marti, J.; Nagy, G.; Guardia, E.; Gordillo, M. C. *J. Phys. Chem. B* **2006**, *110*, 23987–23994.